

ORIGINAL ARTICLE

Rotation of solar-like stars in the immediate solar neighborhood

Jürgen H. M. M. Schmitt | Marco Mittag

Hamburger Sternwarte, Hamburg,
Germany**Correspondence**Jürgen H. M. M. Schmitt, Hamburger
Sternwarte, D-21029 Hamburg, Germany.
Email: jschmitt@hs.uni-hamburg.de**Funding information**Deutsche Forschungsgemeinschaft;
University of Hamburg**Abstract**

Although photometric space-based missions such as CoRoT or *Kepler* have yielded rotation measurements of many thousands of late-type stars during the last decade, the rotational properties of the bulk of the G star population remain undetected by these missions. From the Sun (when viewed as a star), we know that rotation measurements in the ultraviolet are the most promising, or more general, measurements in wavelength regions very sensitive to plage areas on the stars. Therefore, the “classical” S-index, that is, the strength of the Ca II H&K line core emission, is still the most viable activity and rotation indicator, and with robotic spectroscopy telescopes, such monitoring measurements can be carried out efficiently and economically. We define a complete volume-limited sample of solar stars in the immediate solar environment and present period measurements in Ca II H&K, both from archival Mount Wilson data and new data obtained with our robotic TIGRE facility.

KEYWORDS

robotic spectroscopy, rotation periods, stellar activity

1 | INTRODUCTION AND OVERVIEW

While mass is the decisive parameter that governs the position of a star in the Hertzsprung-Russell diagram, rotation is the key parameter for the “magnetic activity” of a given star. By “magnetic activity,” we subsume a plethora of phenomena observed in cool stars, such as star spots, chromospheres, and coronae, more or less across the whole electromagnetic spectrum from radio to X-ray wavelengths. As defined by Linsky (1985), these activity phenomena occur when “the energy balance in a stellar

atmosphere departs greatly from pure radiative equilibrium”; hence, some nonradiative heating processes must be at work.

“Magnetic activity” is typically observed in cool stars with turbulent outer convection zones, and the common paradigm attributes the observed activity to magnetic fields generated by dynamo action in outer envelopes of these stars by a not terribly well-understood interplay between turbulence and convection. At the same time, magnetic activity does lead to angular momentum loss in the form of an ionized magnetic wind as first outlined by Weber & Davis Jr. (1967), which leads to a

gradual spin-down of stars during their lifetimes. In this way, rotation, age, and activity are connected together in the so-called “rotation-age-activity connection,” a central paradigm of the research field “cool star activity.” For these reasons, it is obvious that knowledge of rotation is fundamental for any understanding of stellar activity.

2 | LESSONS FROM THE SUN

The solar rotation has been known ever since Scheiner and Galilei carried out telescopic observations of the Sun in the years 1610–1612 and realized that the apparent motion of the Sun spots is actually caused by the rotation of the whole Sun. Many years of Sun spot observations finally led to the differential rotation law of the Sun (cf., Newton & Nunn (1951)), namely,

$$\Omega(\phi) = 14.38 - 2.44\sin^2(\phi)(\text{deg/day}), \quad (1)$$

where ϕ denotes solar latitude; for a detailed historical perspective, see the overview by Paternò (2010).

For stars, it is usually not possible to obtain spatially resolved surface observations; hence, the question arises as to whether the solar rotation (and solar differential rotation) can also be measured in integrated light and which wavelength range is the best to use. This issue has been addressed by Hempelmann and collaborators in a series of papers. Hempelmann & Donahue (1997) investigate the temporal behavior of the Ca II H&K emission (in the form of the S-index) and demonstrate that the recorded time series shows power at the expected frequencies and even allows an assessment of the differential rotation of the Sun. Observations in white light, that is, in terms of total solar irradiance (TSI), however, do not normally reveal the rotation of the Sun as shown by Hempelmann (2003); only under lucky circumstances near solar minimum conditions did the TSI light curves studied by Hempelmann (2003) show power at the expected frequencies. On the other hand, in solar ultraviolet data in the Mg II h+k and Lyman α lines, Hempelmann (2002) finds an even stronger rotational signal than in the Ca II data, yet these data can only be derived from space-based observations.

The solar TSI record is naturally broadband in its extreme. As discussed by Willson (1997), the TSI varies both by Sun spots rotated onto the visible hemisphere, which cause TSI depressions, and faculae, which cause TSI brightenings, so that the overall signal is a complex interplay of the two effects. These circumstances are illustrated by the image of the Sun displayed in Figure 1. In the core of the Ca II K line, the “quiet” photospheric solar background is very low, leading to a large contrast between the facular,

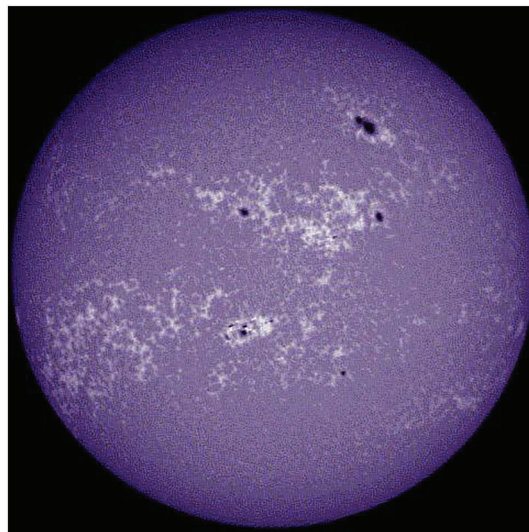


FIGURE 1 The Sun seen in the core of the Ca II K line; Image credit: NASA Marshall Space Flight Center

“active” regions and the nonactive regions. It is also clear that the filling factor of the spots is much smaller than those of the faculae. Only when either spots dominate, as is the case in very active stars, or when faculae dominate, as is sometimes the case in inactive stars, do the resulting light curves show rotational modulation at the correct period (Hempelmann 2003).

3 | PHOTOMETRY: WHAT IS POSSIBLE FROM THE GROUND?

Radick et al. (2018) provide a concise summary of 35 years of photometry of solar-like stars and succinctly point out the limitations of ground-based photometry: Achieving and maintaining the precision needed for stellar observations to make a meaningful comparison to the Sun is next to impossible. The typical precision achievable from traditional photoelectric photometry is about 0.1% for individual observations, and more modern charge coupled device observations reach similar limits for various instrumental (e.g., flat-fielding) and physical (e.g., scintillation) reasons, thus staying about two orders of magnitude worse than state-of-the-art solar observations. Furthermore, achieving stellar observations on any given star with the same cadence as solar observations is again next to impossible in practical terms, and thus, Radick et al. (2018) conclude that “there will probably never be stellar time series with the duration, dense coverage, and the astounding photometric precision of the solar observations (...) for many, or perhaps even any, Sun-like stars, absent a dedicated, coordinated, long-term ground- and space-mission to obtain the needed spectroscopic and photometric data.”

While space-based photometry (cf., Section 4) increases the achievable accuracy by at least one order of magnitude, the limitations are cost and duration, and the vast majority of space missions have lifetimes shorter, and often considerably shorter, than typical solar or stellar cycles.

4 | PHOTOMETRY: THE COROT AND KEPLER REVOLUTION

The advent of the CoRoT (Auvergne et al. 2009) and *Kepler* (Borucki et al. 2011) space missions has revolutionized the photometry of stars. With CoRoT, and later *Kepler*, astronomers had access to essentially uninterrupted light curves over a time scale of a couple of months (typically 120 days), and with *Kepler*, that time span was extended to 4 years. With such datasets, the determination of variability, especially of rotation rates for stars, was made on a sound basis. The new data do not have the typical data gaps that hamper ground-based time series, such as the unavoidable day–night cycle, bad weather periods, or other causes.

The most comprehensive study of stellar rotation periods based on data from the *Kepler* mission is that of McQuillan et al. (2014), who analyzed 3 years of *Kepler* data for 133,030 main sequence stars. In a quarter of the studied stars (more precisely 34,030 stars), these authors were able to determine periods between 0.2 and 70 days. The fundamental result of the study of McQuillan et al. (2014) is shown in Figure 2, where period versus B-V color is shown for the 34,030 rotation periods derived from the *Kepler* data; for more details, we refer to the paper by McQuillan et al. (2014). Note that Figure 2 presents the periods as a function of B-V color rather than mass as in the paper by McQuillan et al. (2014). Figure 2 demonstrates that the bulk of the rotation periods determined from the *Kepler* data is—somewhat dependent on spectral type—below 20–25 days. Furthermore, there appears to exist an upper envelope to the period distribution, which appears to be connected to the convective turnover time. The three red curves are the convective turnover times as given by Cranmer & Saar (2011) (red dotted line, their eq. 36); the convective turnover times as given by Noyes et al. (1984) (red dashed line, their eq. 4 multiplied by a factor of 2); and the convective turnover times as given by Mittag et al. (2018) (red solid line, their eq. 11 and 12). This alignment between the upper period envelope and the convective turnover time is discussed in more detail by Mittag et al. (2018); we also note that Matt et al. (2015) show that this upper envelope agrees with the period distribution calculated in a “synthetic” cluster with an age of 4 Gyrs (cf., Figure 3 in the paper by Matt et al. (2015)).

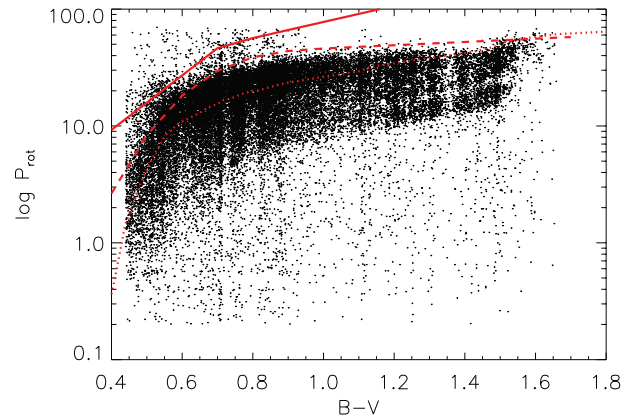


FIGURE 2 Rotation period versus B-V color for *Kepler* stars with periods determined by McQuillan et al. (2014); red lines are convective turnover times calculated from various descriptions (see text for details)

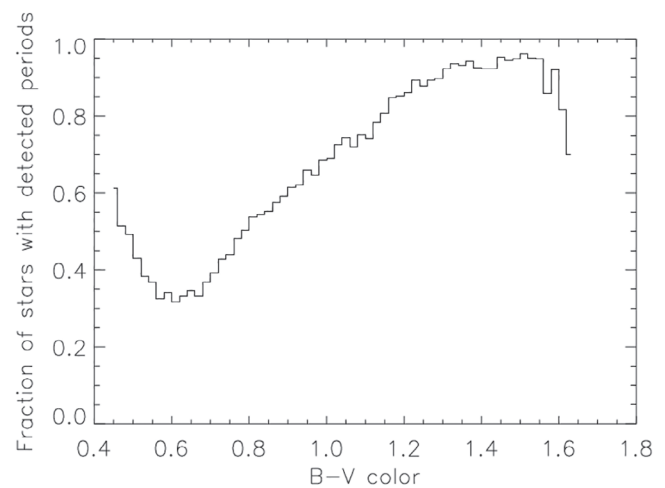


FIGURE 3 Fraction of stars with nondetected period among the stars studied by McQuillan et al. (2014) versus B-V color

It is interesting to inspect those 99,000 stars, for which McQuillan et al. (2014) were unable to extract periods despite the availability of superb *Kepler* data. In Figure 3, we plot the fraction of the stellar population, for which McQuillan et al. (2014) reported successful period measurements. As is clear from Figure 3, for very late-type stars, this fraction approaches 100%; however, for truly solar-like, presumably low-activity stars, this fraction is only about a third, and we conclude that the rotation periods of the bulk of the G-star population observed by *Kepler* remain unknown. In this context, we would, however, like to add two caveats: First, the selection bias of the *Kepler* data is not entirely clear, and second, with increasing rotation period, we expect the stars to become less active and less spot-dominated, so there might be an unknown observational bias in Figure 2.

5 | MEASUREMENT OF ROTATIONAL MODULATION IN CA H&K

Any inhomogeneities present on the stellar surface (cf., Figure 1) can give rise to rotational modulation in suitable activity indicators. On the Sun, chromospherically active plage regions, which are readily seen, for example, in the line cores of the Ca II H&K lines, are often inhomogeneously distributed on the surface and therefore lead to rotational modulation. The same effect should occur on stars, and thus, rotational modulation should also be visible, for example, in the variability of the so-called S-index, which measures the strength of the emission cores in the Ca II H&K lines with regard to the surrounding continuum emission. It is worth pointing out in this context that these line core emission reversals in Ca II H&K seem to have first been described by Eberhard & Schwarzschild (1913) in Potsdam.

The determination of rotational modulation from S-indices was considered on the basis of the Mount Wilson data by Vaughan et al. (1981) and Baliunas et al. (1985) among others. For a subsample of stars in the Mount Wilson sample, nightly observations were scheduled, and the results are reported by Vaughan et al. (1981) and Baliunas et al. (1985).

In Table 1 in Baliunas et al. (1985), one finds the number of data points in each season, and an inspection of those numbers reveals that, for a sample of stars, data could be obtained typically every other day, and in Tables 2 and 3, Baliunas et al. (1985) list their results for 47 main-sequence stars and eight giants. For 27 (of 47) main-sequence stars, a rotation period is listed with typical values between 10 and 20 days, and a few stars show longer periods. In a few cases, Donahue et al. (1996) could demonstrate the possible occurrence of differential stellar rotation. Thus, the Mount Wilson data do indeed show that solar-like rotation can be determined using S-index variations, yet the observational effort is substantial and requires data collection over long periods of time. The Hamburg group has also begun measuring rotation periods in Ca II H&K ever since the inauguration of the TIGRE facility (cf., Section 6), and the first results have been presented by Hempelmann et al. (2016).

6 | MONITORING WITH TIGRE

Imaging, spectroscopy, and monitoring are among the classic tasks of observational astronomy. As astronomers cannot truly experiment with their objects of investigation, monitoring (often over long time scales) plays an important role because only systematic observations reveal

TABLE 1 The TIGRE sample of solar neighborhood solar-like stars

HD number	m_V	B-V	d (pc)	Sp. type	MW
HD10086	6.60	0.690	21.4	G5IV	
HD10307	4.96	0.618	12.6	G2V	Y
HD11131	6.72	0.654	23.0	G0	
HD12846	6.89	0.662	23.2	G2V	
HD18757	6.64	0.634	22.9	G4V	
HD20630	4.84	0.681	9.2	G5Vvar	Y
HD25680	5.90	0.620	16.7	G5V	Y
HD26913	6.94	0.680	20.9	G5IV	
HD30495	5.49	0.632	13.3	G3V	Y
HD32923	4.91	0.657	15.9	G4V	
HD34411	4.69	0.630	12.6	G0V	Y
HD38858	5.97	0.639	15.6	G4V	Y
HD42618	6.85	0.642	23.1	G4V	
HD42807	6.43	0.663	18.1	G8V	Y
HD51419	6.94	0.620	24.2	G5V	
HD63433	6.90	0.682	21.8	G5IV	
HD67228	5.30	0.642	23.3	G2IV	
HD68017	6.78	0.679	21.7	G4V	Y
HD71148	6.32	0.624	21.8	G5V	Y
HD72905	5.63	0.618	14.3	G1.5Vb	
HD73350	6.74	0.655	23.6	G0	
HD75767	6.57	0.640	24.1	G0	Y
HD76151	6.01	0.661	17.1	G3V	Y
HD84737	5.08	0.619	18.4	G2V	
HD86728	5.37	0.676	14.9	G1V	Y
HD89269	6.66	0.653	20.6	G5	Y
HD92719	6.79	0.622	23.4	G2/G3V	
HD95128	5.03	0.624	14.1	G0V	Y
HD126053	6.25	0.639	17.6	G1V	Y
HD133640	4.83	0.647	12.8	G2V + G2V	Y
HD139777	6.57	0.665	22.1	G8IV-V+...	
HD140538	5.86	0.684	14.7	G5V	
HD143761	5.39	0.612	17.4	G2V	Y
HD146233	5.49	0.652	14.0	G1V	

the behavior of a given source in the time domain and may reveal the underlying physical processes. The longest known astronomical time series is probably that of the Sun spot cycle, which dates back to the times of Galileo and Scheiner in 1610. The availability of photometry on archival photographic plates allows the construction of

TABLE 2 TIGRE period measurements

HD number	Season	N_{obs}	S-index	Dispersion	$P_{\text{GP}} \pm P_{\text{GP, err}}$ (days)	$P_{\text{GP, Like}}$	$P_{\text{GLS}} \pm P_{\text{GLS, err}}$ (days)	$P_{\text{GLS, FAP}}$
HD10086	2015	18	0.294	0.008	13.06 ± 0.30	2.13	13.07 ± 0.31	0.15
HD10086	2017/18	22	0.297	0.012	13.75 ± 0.21	6.21	13.70 ± 0.14	0.0005
HD12846	2015	16	0.161	0.002	29.69 ± 0.94	2.33	29.81 ± 1.02	0.06
HD20630	2015/16	16	0.352	0.061	9.10 ± 0.13	2.59	9.09 ± 0.12	0.05
HD25680	2014	17	0.317	0.006	10.51 ± 0.59	1.13	10.23 ± 0.67	0.11
HD25680	2014/15	35	0.317	0.006	10.52 ± 0.13	15.9	10.53 ± 0.07	0.0
HD25680	2015/16	19	0.311	0.008	10.91 ± 0.31	1.59	10.79 ± 0.25	0.19
HD30495	2013/14	35	0.281	0.009	12.01 ± 0.38	5.15	11.72 ± 0.16	0.004
HD30495	2014/15	48	0.317	0.012	11.11 ± 0.17	14.64	11.26 ± 0.08	0.00
HD30495	2015/16	21	0.288	0.006	11.07 ± 0.13	4.25	11.05 ± 0.13	0.009
HD30495	2014/15	48	0.317	0.012	11.11 ± 0.17	14.64	11.26 ± 0.08	0.00
HD32923	2014/15	26	0.146	0.002	30.63 ± 0.23	1.03	30.78 ± 1.03	0.19
HD32923	2017/18	25	0.141	0.006	34.90 ± 2.28	1.47	35.16 ± 2.40	0.21
HD32923	2018/19	47	0.141	0.006	10.67 ± 0.19	3.09	10.69 ± 0.13	0.0068
HD38858	2014	16	0.177	0.003	17.97 ± 0.70	2.64	17.75 ± 0.82	0.02
HD38858	2014/15	24	0.173	0.002	50.40 ± 1.94	2.41	49.99 ± 2.08	0.035
HD38858	2015/16	22	0.165	0.002	48.50 ± 2.43	2.12	49.60 ± 2.50	0.05
HD42807	2013/14	32	0.363	0.009	11.80 ± 0.12	7.63	11.80 ± 0.08	0.0001
HD42807	2014/15	31	0.368	0.007	10.49 ± 0.20	1.45	10.47 ± 0.30	0.11
HD42807	2018/19	18	0.373	0.014	11.95 ± 0.26	3.15	12.01 ± 0.22	0.012
HD71148	2018/19	31	0.157	0.005	23.08 ± 0.93	1.58	23.21 ± 1.00	0.036
HD72905	2013/14	49	0.398	0.009	5.23 ± 0.02	8.93	5.23 ± 0.03	0.0001
HD72905	2014/15	50	0.410	0.010	4.88 ± 0.11	4.03	5.04 ± 0.04	0.186
HD72905	2015/16	19	0.395	0.012	3.18 ± 0.03	2.73	3.19 ± 0.01	0.045
HD72905	2017/18	35	0.369	0.011	4.77 ± 0.10	2.83	4.70 ± 0.02	0.084
HD72905	2018/19	17	0.357	0.008	4.89 ± 0.06	1.57	4.90 ± 0.03	0.120
HD76151	2015/16	15	0.245	0.004	27.81 ± 1.71	1.68	30.67 ± 1.12	0.052
HD76151	2018/19	29	0.226	0.008	15.54 ± 0.42	1.70	15.62 ± 0.30	0.149
HD84737	2014/15	47	0.141	0.002	42.42 ± 1.37	3.20	42.98 ± 1.76	0.015
HD86728	2014/15	43	0.149	0.003	23.23 ± 0.59	2.44	23.27 ± 0.65	0.021
HD86728	2015/16	23	0.145	0.004	20.82 ± 0.70	1.62	20.66 ± 0.79	0.144
HD86728	2018/19	35	0.143	0.003	12.06 ± 0.34	2.79	12.12 ± 0.25	0.021
HD89269	2015/16	18	0.160	0.002	18.39 ± 0.49	1.16	18.30 ± 0.44	0.238
HD95128	2014	38	0.154	0.004	24.38 ± 0.86	1.73	25.04 ± 1.24	0.150
HD95128	2014/15	44	0.154	0.002	12.14 ± 0.27	1.21	12.11 ± 0.23	0.201
HD126053	TBD	24	0.165	0.003	10.66 ± 0.26	1.15	10.62 ± 0.21	0.036
HD126053	2019	61	0.162	0.005	15.74 ± 0.35	2.53	15.72 ± 0.33	0.013
HD140538	2015	53	0.238	0.004	25.98 ± 1.35	1.43	25.76 ± 1.49	0.035
HD140538	2017	70	0.236	0.009	21.08 ± 0.64	2.06	21.09 ± 0.50	0.007
HD140538	2018/19	75	0.201	0.008	21.08 ± 1.11	3.29	22.23 ± 0.45	0.056
HD143761	2017	39	0.146	0.002	14.84 ± 0.35	1.45	14.84 ± 0.39	0.152
HD146233	2014	34	0.171	0.004	8.63 ± 0.15	2.04	8.64 ± 0.08	0.076
HD146233	2015	25	0.166	0.003	22.93 ± 0.82	1.69	22.88 ± 0.99	0.182
HD146233	2016	16	0.161	0.003	9.10 ± 0.20	2.16	9.13 ± 0.25	0.025

TABLE 3 Mount Wilson period measurements

HD number	Season	N_{obs}	S-index	Dispersion	$P_{\text{GP}} \pm P_{\text{GP, err}}$ (days)	$P_{\text{GP, Like}}$	$P_{\text{GLS}} \pm P_{\text{GLS, err}}$ (days)	$P_{\text{GLS, FAP}}$
HD20630	1967/68	17	0.406	0.014	8.89 ± 0.11	4.55	8.89 ± 0.05	0.004
HD20630	1968/69	14	0.367	0.017	13.72 ± 0.21	2.76	13.65 ± 0.09	0.032
HD20630	1980/81	82	0.352	0.009	9.20 ± 0.14	9.84	9.18 ± 0.08	0.0001
HD20630	1981/82	34	0.336	0.010	9.21 ± 0.34	5.35	9.03 ± 0.24	0.0004
HD20630	1984/85	59	0.356	0.012	10.56 ± 0.14	3.21	10.57 ± 0.09	0.013
HD20630	1985/86	58	0.341	0.008	9.15 ± 0.10	4.56	9.16 ± 0.06	0.0004
HD20630	1986/87	49	0.341	0.012	9.45 ± 0.08	8.43	9.47 ± 0.08	0.00005
HD20630	1987/88	62	0.329	0.011	9.57 ± 0.16	2.04	9.54 ± 0.09	0.061
HD20630	1988/89	45	0.345	0.007	9.51 ± 0.17	1.90	9.49 ± 0.11	0.057
HD20630	1989/90	26	0.370	0.009	9.47 ± 0.15	3.69	9.48 ± 0.09	0.0029
HD20630	1990/91	25	0.364	0.014	9.09 ± 0.11	8.88	9.07 ± 0.06	0.00002
HD20630	1991/92	21	0.355	0.011	9.10 ± 0.39	1.91	9.17 ± 0.14	0.0054
HD20630	1992/93	35	0.337	0.013	9.16 ± 0.07	10.15	9.15 ± 0.05	0.00001
HD20630	1993/94	28	0.327	0.012	9.03 ± 0.09	8.95	9.02 ± 0.07	0.00001
HD20630	1994/95	42	0.331	0.012	9.09 ± 0.09	18.03	9.02 ± 0.04	0.0
HD26913	1987/88	53	0.348	0.010	12.74 ± 0.15	2.19	12.74 ± 0.18	0.059
HD26913	1988/89	47	0.354	0.015	16.19 ± 0.54	1.22	16.19 ± 0.55	0.147
HD26913	1994/95	52	0.384	0.012	28.99 ± 0.09	1.75	29.07 ± 1.40	0.082
HD43587	1993/94	39	0.152	0.003	26.38 ± 4.26	1.09	26.58 ± 0.95	0.012
HD71148	1993/94	16	0.153	0.004	31.28 ± 0.75	2.51	31.22 ± 0.76	0.021
HD76151	1980/81	38	0.261	0.006	11.34 ± 0.19	2.12	11.36 ± 0.16	0.066
HD76151	1981/82	28	0.234	0.006	14.90 ± 0.27	2.10	14.83 ± 0.24	0.043
HD76151	1985/86	30	0.226	0.005	16.15 ± 0.53	1.70	16.11 ± 0.38	0.0078
HD76151	1987/88	47	0.219	0.004	14.81 ± 0.30	1.85	14.76 ± 0.19	0.0003
HD76151	1993/94	45	0.239	0.006	15.24 ± 0.18	7.76	15.16 ± 0.17	0.00006
HD76151	1994/95	31	0.262	0.008	36.95 ± 1.84	1.58	36.64 ± 1.86	0.071
HD126053	1982	82	0.167	0.005	28.60 ± 0.92	1.13	28.52 ± 0.90	0.203
HD126053	1983	65	0.167	0.003	8.94 ± 0.21	1.03	8.94 ± 0.13	0.248
HD126053	1992	25	0.170	0.003	9.36 ± 0.24	1.02	9.37 ± 0.16	0.018
HD143761	1983	88	0.151	0.004	19.90 ± 0.49	1.57	19.87 ± 0.49	0.120
HD143761	1984	81	0.149	0.005	18.09 ± 0.31	2.99	18.14 ± 0.26	0.021
HD143761	1985	83	0.150	0.002	41.24 ± 2.30	1.90	41.18 ± 1.89	0.00038
HD143761	1986	79	0.149	0.003	49.39 ± 3.50	1.05	49.31 ± 3.58	0.100
HD143761	1987	68	0.149	0.004	17.43 ± 0.31	2.57	17.45 ± 0.31	0.029

light curves over approximately 100 years, albeit the selection of sources is typically quite random, and the data quality is quite mixed and only rarely meets modern standards.

Advances in telescope, computer, and internet technology currently allow the possibility of other

solutions for such repetitive observational tasks as monitoring, which are far more economical and far more efficient than the traditional approach. At Hamburg, we have established TIGRE, that is, Telescopio Internacional de Guanajuato Robótico Espectroscópico, a fully robotic 1.2-m telescope located at the La Luz Observatory

(in central Mexico) of the Department of Astronomy of the University of Guanajuato. The TIGRE project is run by astronomers from Hamburger Sternwarte, from Guanajuato, and the High Energy Astrophysics group of the University of Liège. The TIGRE telescope feeds a high-resolution spectrograph, which covers most of the optical spectrum between 3,800 and 8,900 Å, with a spectral resolving power $\lambda/\Delta\lambda \sim 20,000$. The spectral data are reduced by an automatic data reduction pipeline and are usually available for scientific analysis 1 day after data acquisition. The telescope operation is fully automatic, with the system choosing its targets from an object list based on sky availability and—of course—the priorities set by the observer; a detailed description of the TIGRE facility and its performance is given by Schmitt et al. (2014).

7 | THE TIGRE SAMPLE

In order to address the rotational properties of an unbiased, complete sample of solar-like stars, we select all stars in the color range $0.6 < B-V < 0.7$ and a distance $d < 25$ pc with declinations $\delta > -20^\circ$ and in the right ascension range $1.5 \text{ hr} < \text{RA} < 15.75 \text{ hr}$; the latter restrictions come from the requirement that we preferentially choose winter objects visible from the La Luz site in Guanajuato, Mexico. This leaves us with an—admittedly—small sample of 34 stars listed in Table 1. The advantage of this sample is that it is well observed in other wavelength ranges, and some of the sample stars are also contained in the Mount Wilson sample presented by Baliunas et al. (1995), who present almost 30 years of Ca II monitoring. In fact, for 20 of our 34 sample stars, we also have Mount Wilson data: 6 stars had more than 400 individual observations, 7 stars less than 7 individual observations, and another 7 stars between 30 and 70 individual observations with very different temporal cadences. So, one concludes that the temporal coverage of our sample in the Mount Wilson program was extremely heterogeneous.

8 | TIGRE OBSERVATIONS AND PERIOD ANALYSIS

Naturally, the TIGRE coverage of our sample is also heterogeneous. In addition, with TIGRE, it is not possible to monitor all the sample stars simultaneously as other observation programs are also run, and optimizing our scheduling procedures is a learning experience. As a—more or less—typical example, we show our TIGRE light curve for the star HD12846 obtained in the 2015

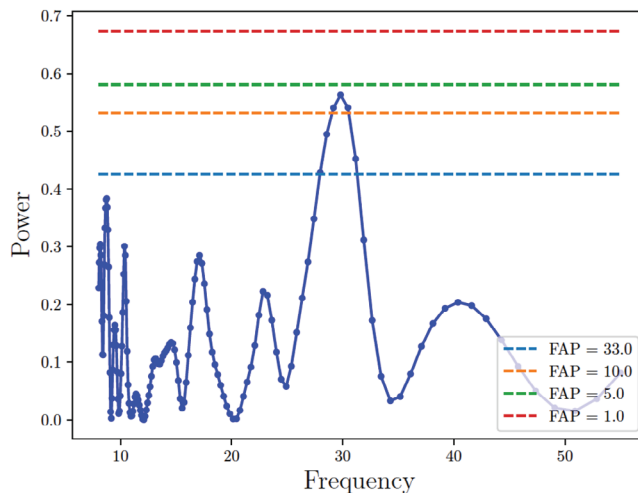


FIGURE 4 Generalized Lomb-Scargle power as a function of period for the TIGRE S-index light curve HD12846 shown in Figure 5. False alarm probability (FAP) values are given at the 25, 10, 5, and 1% levels, that is, the confidence for the shown case is a little below 95%

observing season; the one-season S-index variability is immediately apparent.

To determine periods from the data, we follow the approach adopted by Fuhrmeister et al. (2019) in their search for periodic variability in the CARMENES spectra of M dwarfs. Fuhrmeister et al. (2019) used various period-determination methods, viz. phase dispersion minimization, string length minimization, Lomb-Scargle (LS) periodograms, and Gaussian process (GP) modeling, and found that LS periodograms and GP modeling yield the best results. As our TIGRE light curves are quite similar to the CARMENES light curves, we focus on the latter two methods. We specifically use the generalized GLS periodogram, as implemented in PyAstronomy (<https://github.com/sczesla/PyAstronomy>) (Lomb 1976; Scargle 1982; Zechmeister & Kürster 2009), to compute periodograms for our S-index time series in the range between 8 and 55 days, except for the case of HD72905 where we searched periods as low as 3 days.

An example of a GLS periodogram is shown in Figure 4 for the data for HD12846 displayed in Figure 5. Together with the periodograms, we compute false alarm probability (FAP) levels of 33, 10, 5, and 1%, which are also displayed in Figure 5. As is clear from Figure 5, the dominant peak is located at 30 days; however, its significance (in a single observing season) is a little under 95%.

As described by Rasmussen & Williams (2006), a GP consist of sets of random variables of which any finite set has a joint normal distribution. Therefore, a GP is completely specified by a mean and a covariance function, and the latter can be used to search for periodic variation.

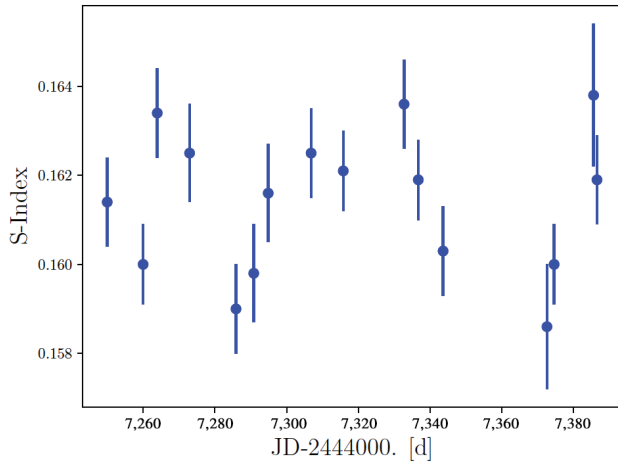


FIGURE 5 TIGRE S-index light curve of HD12846 in the 2015 observing season

At the heart of GP modeling lies the choice of the kernel function, which describes the covariance of the data. This choice of kernel is essentially ad hoc and depends on the data to be modeled. Again following Fuhrmeister et al. (2019), we use a covariance function of the form:

$$k(t_n, t_m) = \frac{a}{2+b} e^{-c\tau} \left[\cos\left(\frac{2\pi\tau}{P}\right) + (1+b) \right] + \delta_{nm}\sigma^2, \quad (2)$$

where $\tau = |t_n - t_m|$, and t_i denotes the individual time stamps. This choice of kernel corresponds to the proposal by Foreman-Mackey et al. (2017) in their eq. 56, extended by a “jitter” term, that is, additional, normally distributed white noise. The kernel defined by Equation (2) is characterized by an exponential decay on time scale τ and includes a periodic term with a period, P , and a secular term. The amplitude of the covariance and the relative impact of the periodic and secular terms are determined by combinations of the values of the parameters b and c ; note that all of the parameters a , b , c , τ , and P must be positive. The main difficulty in GP modeling because the covariance matrix of the data needs to be inverted many times, and the “celerite” algorithm as proposed by Foreman-Mackey et al. (2017) can do this very efficiently.

In our modeling, the four parameters a , b , c , and P are varied to find the maximum of the likelihood function, which is accomplished using the “limited memory Broyden-Fletcher-Goldfarb-Shanno with box constraints” (L-BFGS-B) algorithm, an iterative optimization algorithm belonging to the group of the quasi-Newton methods, as implemented in `SciPy` (Jones et al. 2001). In this way, we can determine—for every choice of period—the best-fitting model parameters and the likelihood for the best-fit model. To compute the significance of a considered model, we determine the likelihood difference between a model with a given period and without any period. For the

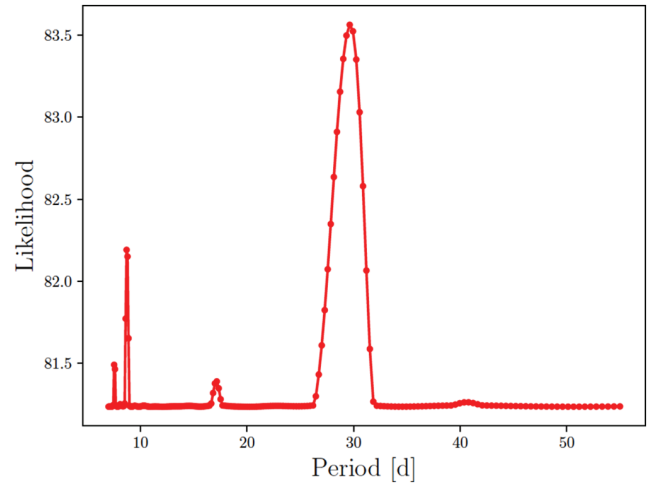


FIGURE 6 Results for the Gaussian process (GP) modeling of the S-index light curve of HD12846 displayed in Figure 5. Shown is the likelihood of a GP model with period P compared to a GP model without any period as a function of the test period

specific case of HD12846, the likelihood difference is displayed in Figure 6, which shows a clear peak at 29.81 days, at almost exactly the same period where we find the largest peak in the GLS periodogram. We are therefore confident that this is actually the correct period for HD12846.

9 | RESULTS

9.1 | TIGRE period measurements

In our analysis, we use only one-season data for our sample stars as a matter of principle. While one could also use data distributed over several seasons, we refrain from using such data as this might cause undesired phase shifts when active regions develop on different parts of the surface. Such a procedure naturally limits the accuracy of the achieved results, and the quoted significance thresholds always refer to a single season. We have refrained from pooling individual seasons; however, it is clear that the period significance increases substantially once independent seasons with comparable period measurements are considered together.

In Table 2, we present the results of our analysis of the TIGRE observations. In Table 2, we specifically provide the star name, the observing season the data row refers to, the number of data points, the mean S-index and its dispersion, the best-fit GP modeling period and its error, the likelihood difference compared to a model without the period term, the best-fit GLS period and its error, and the FAP. Note that we report periods only in those cases where the GP and GLS periods can be derived individually, are consistent with each other, and show a FAP of less

than 25%. We do not provide periods if only one method yields valid results or if the FAP exceeds 25%. We specifically point out that a “no-period measurement” can be due to a small number of data points; however, even a larger number of data points does not necessarily guarantee a successful period measurement. In addition, a 25% FAP threshold is of course extremely low; however, in conjunction with our requirement that GP modeling must yield a comparable period, we are confident that many of our periods are accurate. We specifically performed random permutation of our time series and carried out an identical analysis, which demonstrated that our selection criteria are quite robust but not perfect.

9.2 | Mount Wilson data and period measurements

The data obtained in the context of the Mount Wilson Project have been publicly released and can be downloaded from ftp://solis.nso.edu/MountWilson_HK/. A detailed description of these data is also provided at this website; the available data specifically include the star identification, the calibrated S-index (which we use in this paper as the basis for our analysis), an instrument code indicating with which instrument the data were obtained, and the date of the observation, as well as other material. The Mount Wilson project ran for about 30 years, and tens of thousands of individual observations were made. Naturally, the coverage of individual stars is extremely heterogeneous. Some stars, for example, τ Boo, were observed a few thousand times, while for others, only a few snapshot observations exist, which characterize the overall activity of the star in question but do not allow any meaningful further timing analysis. To determine periods from the Mount Wilson data, we followed the same procedure as for the TIGRE observations and present the corresponding results in Table 3.

10 | DISCUSSION

An inspection of the results given in Tables 2 and 3 shows that, for a significant fraction of the sample stars, rotation periods have been detected; however, in some cases, the results are unfortunately not entirely unambiguous. In Table 4, we therefore provide a—admittedly in parts subjective—summary of what we think the best current period estimates of our sample stars are. For each star, we provide the name, the measured mean S-index, the estimated Rossby number, and the estimated period (in days), as well as a numerical “quality” flag. Here, “1” indicates that we are certain that the period is correct as proven

by independent high-quality measurements; “2” indicates that we are quite confident that the period is correct; “3” indicates a likely period that needs confirmation by further observations; “4” indicates a possible period that is in desperate need of observational confirmation; and “5” indicates that only an estimated period is available (see below). Overall, we find periods (of variable quality) for 60% of our sample, which is a significant improvement over *Kepler*, where periods could be derived only for a third of the G star population (cf., Figure 3).

For a few stars, both TIGRE and Mount Wilson measurements are available: For HD20630, the two period determinations appear to agree reasonably well; however, from Table 3, it is obvious that HD20630 was observed very intensely in the context of the Mount Wilson program. These observations are also discussed by Donahue et al. (1996), who noted period “variations,” albeit not as large as evident in Table 3. These variations appear significant, and the physical reason is unclear. Another star in common is HD71148, which, however, has discrepant period measurements (cf., Table 2 and Table 3) with periods of 23.1 days from TIGRE and 30.3 days from Mount Wilson; we inspected the periodograms, and the derived periods appear to be correct, so further observations of HD71148 are definitely necessary. For the star HD76151, we also have period measurements from TIGRE and Mount Wilson data; interestingly, both datasets show “low” and “high” periods. In many (but not all) periodograms, we find several significant peaks, so again, this star requires further observations. Yet another star in common is HD143761, for which we measure a period of 14.9 days from our TIGRE data with a relatively low FAP, and the inspection of the periodogram shows a second peak near 46 days with almost the same power. HD71148 has been extensively monitored in the Mount Wilson program, and for five seasons, periods could be determined but with different period results (cf., Table 3). One possibility would be to interpret the TIGRE and the low Mount Wilson measurements as an alias of an approximate 40-day period, and obviously, this star also requires further observations.

In Table 4, we also provide “calculated” rotation periods, computed from the mean S-indices provided in the very same table. To estimate the stellar rotation period from the activity level, we use the R_{HK}^+ -Rossby number relation derived by Mittag et al. (2018). The R_{HK}^+ activity index is the pure flux excess described in detail by Mittag et al. (2013); we compute the R_{HK}^+ value for all our sample stars with the observed mean S_{MWO} derived from our TIGRE data and the $T_{\text{eff}}(B - V)$ relation from Gray (2005, eq. 14.17). We then estimate the Rossby numbers from our derived R_{HK}^+ values, and finally, to obtain the estimated rotation period, we multiply the Rossby number

TABLE 4 Summary: Rotation periods of solar neighborhood solar-like stars

HD number	S-index	Rossby number	P_{calc} (days)	P_{obs} (days)	Quality
HD10086	0.294	0.35	15.3 ± 0.5	13.6	1
HD10307	0.150	0.56	25.4 ± 1.1	n.a.	5
HD11131	0.329	0.28	10.0 ± 0.4	n.a.	5
HD12846	0.160	0.79	29.7 ± 1.1	29.6	2
HD18757	0.350	0.24	7.66 ± 0.4	n.a.	5
HD20630	0.364	0.24	10.0 ± 0.4	9.15	1
HD25680	0.316	0.28	8.5 ± 0.4	10.5	1
HD26913	0.382	0.21	8.9 ± 0.5	13	3
HD30495	0.289	0.33	10.7 ± 0.5	11.1	1
HD32923	0.144	0.90	32.9 ± 1.5	32	3
HD34411	0.147	0.88	27.9 ± 1.2	n.a.	5
HD38858	0.169	0.73	24.4 ± 1.0	48	3
HD42618	0.163	0.77	26.0 ± 1.1	n.a.	5
HD42807	0.364	0.23	8.7 ± 0.3	11.8	1
HD51419	0.172	0.71	21.4 ± 0.8	n.a.	5
HD63433	0.386	0.21	8.8 ± 0.4	n.a.	5
HD67228	0.136	0.97	32.8 ± 1.5	n.a.	5
HD68017	0.171	0.73	30.1 ± 1.25	n.a.	5
HD71148	0.160	0.78	24.1 ± 1.0	23.1	2
HD72905	0.393	0.16	4.8 ± 0.3	4	2
HD73350	0.274	0.37	13.6 ± 0.5	n.a.	2
HD75767	0.247	0.43	14.4 ± 0.5	n.a.	5
HD76151	0.230	0.49	18.2 ± 0.7	16	3
HD84737	0.140	0.94	28.1 ± 1.3	40.5	2
HD86728	0.147	0.87	35.5 ± 1.6	23	3
HD89269	0.159	0.79	28.5 ± 1.2	19	3
HD92719	0.177	0.69	20.9 ± 0.8	n.a.	5
HD95128	0.149	0.86	26.5 ± 1.2	24	3
HD126053	0.166	0.75	25.1 ± 1.0	15.8	2
HD133640	0.244	0.44	15.3 ± 0.5	n.a.	5
HD139777	0.325	0.29	11.1 ± 0.5	n.a.	5
HD140538	0.232	0.49	20.8 ± 0.7	21.2	2
HD143761	0.146	0.88	25.5 ± 1.1	14.8	3
HD146233	0.162	0.77	27.7 ± 1.2	20	4

values with the corresponding values for the convective turnover time, which in turn is calculated from the convective turnover time relation derived by Mittag et al. (2018), and list our final values in Table 4; we note again that these values represent our—possibly subjective—judgments of the actual periods.

In quite a few cases, the observed and calculated periods agree well or reasonably well; however, in a few cases, these two periods differ significantly. In the case of HD26913, the S-index values of our TIGRE measurements are consistent with those derived from the Mount data; however, the TIGRE cadence is insufficient for a period determination. HD26913 has been intensely observed in the context of the Mount Wilson program; in some seasons, more than 60 individual observations were taken, but the period determinations (cf., Table 3) are—usually—not that significant and, even worse, discrepant, so we must leave the “correct” period open. In the case of HD32923, two of our successful seasons yield periods at the “expected” value, albeit with rather low significance, and our period for HD32923 with the best significance does not fit the very low S-index observed at all, so further observations of this star are necessary. In the case of HD38858, the situation is similar; our three seasons yield discrepant results, and none of our periods agrees with the “expected period”; thus, further observations of HD38858 are clearly necessary. In the case of HD84737, our best season (with 47 individual measurements) results in a clear period, and we find no signal at the “expected” 28-day period, but a confirmation of the observed period would be desirable. In the case of HD86728, none of our periods are even close to the “expected” 35-day period, but again, a confirmation of the observed period would be desirable. In the case of HD89269, the derived period is of very low significance, so one should not overrate the “contradiction” to the calculated period. The case of HD126053 appears to also be peculiar. In the Mount Wilson data, periods could be derived for three seasons, yet with discrepant values; the period derived for the 1982 season is close to expectations, but the FAP of this period is quite large, while the other periods are far too low given the small S-index of HD126053. In addition, our TIGRE periods are not even close to the “expected” 25-day period, so the value of the correct observed period is open. HD143761 has been intensely observed in the Mount Wilson program, yet the derived periods are again discrepant, and none of these periods corresponds to expectations. Our best TIGRE season yields an even shorter period, so again, the value of the correct observed period remains open. Finally, in the case of HD146233, we have discrepant period determinations. One season is marginally close to expectations; however, this period determination has very low significance. Our period determinations with high significance yield much lower periods, which do not really agree with the moderate activity level of HD146233.

Further inspection of Table 4 shows that not all of the stars with no or unreliable periods (i.e., quality measures “4” and “5”) are of low activity, where period measurements are cumbersome. A few stars, for example,

HD18757 or HD63433, are actually quite active, and it is a little surprising that our Ca monitoring resulted in no detections. For those objects, photometric periods might be obtained, for example, from TESS observations. We plan to continue our program focusing on the less active stars without reliable period estimates.

ACKNOWLEDGMENTS

We acknowledge the continued support by various partners who helped realize and run TIGRE. We thank the University of Hamburg, which gave support in terms of funding, manpower, and workshop resources. Furthermore, grants from the Deutsche Forschungsgemeinschaft (DFG) in various funding lines are gratefully acknowledged, as well as travel money from the DFG, DAAD, and Conacyt in several bilateral grants. The HK_Project_v1995_NS0 data are derived from the Mount Wilson Observatory HK Project, which was supported by both public and private funds through the Carnegie Observatories, the Mount Wilson Institute, and the Harvard-Smithsonian Center for Astrophysics, starting in 1966 and continuing for over 36 years. These data are the result of the dedicated work of O. Wilson, A. Vaughan, G. Preston, D. Duncan, S. Baliunas, and many others. We also acknowledge very helpful discussions on convective turnover times and rotation periods with S. Matt. Open access funding enabled and organized by Projekt DEAL.

REFERENCES

- Auvergne, M., Bodin, P., Boissard, L., et al. 2009, *A&A*, 506, 411.
- Baliunas, S. L., Horne, J. H., Porter, A., et al. 1985, *ApJ*, 294, 310.
- Baliunas, S. L., Donahue, R. A., Soon, W. H., et al. 1995, *ApJ*, 438, 269.
- Borucki, W. J., Koch, D. G., Basri, G., et al. 2011, *ApJ*, 728, 117.
- Cranmer, S. R., & Saar, S. H. 2011, *ApJ*, 741, 54.
- Donahue, R. A., Saar, S. H., & Baliunas, S. L. 1996, *ApJ*, 466, 384.
- Eberhard, G., & Schwarzschild, K. 1913, *ApJ*, 38, 292.
- Foreman-Mackey, D., Agol, E., Ambikasaran, S., & Angus, R. 2017, *AJ*, 154, 220.
- Fuhrmeister, B., Czesla, S., Schmitt, J. H. M. M., et al. 2019, *A&A*, 623, A24.
- Gray D. F. 2005, oasp.book.
- Hempelmann, A. 2002, *A&A*, 388, 540.
- Hempelmann, A. 2003, *A&A*, 399, 717.
- Hempelmann, A., & Donahue, R. A. 1997, *A&A*, 322, 835.
- Hempelmann, A., Mittag, M., Gonzalez-Perez, J. N., Schmitt, J. H. M. M., Schröder, K. P., & Rauw, G. 2016, *A&A*, 586, A14.
- Jones, E., Oliphant, T., & Peterson, P. 2001, SciPy: Open source scientific tools for Python. Retrieved from <http://www.scipy.org/>
- Linsky, J. L. 1985, *SoPh*, 100, 333.
- Lomb, N. R. 1976, *Ap&SS*, 39, 447.
- Matt, S. P., Brun, A. S., Baraffe, I., Bouvier, J., & Chabrier, G. 2015, *ApJL*, 799, L23.
- McQuillan, A., Mazeh, T., & Aigrain, S. 2014, *ApJS*, 211, 24.
- Mittag, M., Schmitt, J. H. M. M., & Schröder, K.-P. 2013, *A&A*, 549, A117.
- Mittag, M., Schmitt, J. H. M. M., & Schröder, K.-P. 2018, *A&A*, 618, A48.
- Newton, H. W., & Nunn, M. L. 1951, *MNRAS*, 111, 413.
- Noyes, R. W., Hartmann, L. W., Baliunas, S. L., Duncan, D. K., & Vaughan, A. H. 1984, *ApJ*, 279, 763.
- Paternò, L. 2010, *Ap&SS*, 328, 269.
- Radick, R. R., Lockwood, G. W., Henry, G. W., Hall, J. C., & Pevtsov, A. A. 2018, *ApJ*, 855, 75.
- Rasmussen C. E., & Williams C. K. I. 2006, gpml.book.
- Scargle, J. D. 1982, *ApJ*, 263, 835.
- Schmitt, J. H. M. M., Schröder, K.-P., Rauw, G., et al. 2014, *Astron. Nachr.*, 335, 787.
- Vaughan, A. H., Preston, G. W., Baliunas, S. L., Hartmann, L. W., Noyes, R. W., Middelkoop, F., & Mihalas, D. 1981, *ApJ*, 250, 276.
- Weber, E. J., & Davis, L. Jr. 1967, *ApJ*, 148, 217.
- Willson, R. C. 1997, *Science*, 277, 1963.
- Zechmeister, M., & Kürster, M. 2009, *A&A*, 496, 577.

How to cite this article: Schmitt JHMM, Mittag M. Rotation of solar-like stars in the immediate solar neighborhood. *Astron. Nachr.* 2020;341:497–507. <https://doi.org/10.1002/asna.202013790>